Supplementary Information

Supplementary Figure 1; Evaluation of *in vivo* stoichiometry of Cks1 in cyclin-Cdk1 complexes and of the ability of Cks1 to bind the phosphorylated Sic1∆C.

Supplementary Figure 2; Analysis of the processivity of Sic1∆C multiphosphorylation.

Supplementary Figure 3; Simulation of the multiphosphorylation time courses.

Supplementary Figure 4; Analysis of Sic1 phosphorylation and degradation.

Supplementary Figure 5; Analysis of Cks1-dependent phosphorylation of the 'non-Cdk' site T48 using quantitative mass-spectrometry.

Supplementary Figure 6; Phosphorylation-dependent enhancement of secondary phosphorylation steps in substrate constructs containing two phosphorylation sites.

Supplementary Figure 7; Effects of Sic1∆N overexpression on levels of Cln2 and Clb5.

Supplementary Figure 8; A schematic diagram describing the prevalent routes of Cln2- and Clb5-dependent multi-phosphorylation of Sic1.

Supplementary Equations

Supplementary Discussion

Supplementary Tables 1 and 2; Docking constants (k_{dock}) determined for pairs of Cdk1 phosphorylation sites.

Supplementary Table 3; Yeast strains used in this study.

Supplementary Table 4; Plasmids used in this study.

Supplementary equations

Comparison of processive and distributive mechanism at varied substrate concentrations (Supplementary Fig. 2e)

Simulation for Supplementary Fig. 2e:
y(1) = S0; y(2) = S1P; y(3) = S2P; y(4) = S3P; y(5) = S4P; y(6) = S5P; y(7) = S6P;

k1=10; kcat for S0 to S1P transition
k2=10; kcat/KM for S1P to S2P transition
k3=10; kcat/KM for S2P to S3P transition
k4=10; kcat/KM for S3P to S4P transition
k5=10; kcat/KM for S4P to S5P transition
k6=10; kcat/KM for S5P to S6P transition
k7=10; KM for S0
k8=3 or 0.75; factor by which S0 exceeds the KM

```
dydt = [(-k1*(k7*k8-y(2)-y(3)-y(4)-y(5)-y(6)-y(7)))/(k7+(k7*k8-y(2)-y(3)-y(4)-y(5)-y(6)-y(7)))
       (k1*y(1))/(k7+y(1))-k2*y(2)/(1+y(1)/k7)
       (k2*y(2)-k3*y(3))/(1+y(1)/k7)
       (k3*y(3)-k4*y(4))/(1+y(1)/k7)
       (k4*y(4)-k5*y(5))/(1+y(1)/k7)
       (k5*y(5)-k6*y(6))/(1+y(1)/k7)
       (k6*y(6))/(1+y(1)/k7)];
```

The initial values for S0 in two simulations were 30 and 7.5 (substrate concentrations of 0.75xKM and 3xKM). It was assumed that within the initial product accumulation range that was followed, for any intermediates SnP $<<KM_{SnP}$ was true. The simulations were performed using the MATLAB ode45 solver. For the diagram presented in Supplementary Figure 2e, the two time points mimicking the aliquots taken at 2.5 and 5 minutes in the experiment (Supplementary Fig. 4i) were taken at the points around 1.5% and 3% of the total turnover of the substrate, calculated from the simulation with a substrate concentration of 3xKM. The same time points were used to get the vaules from the simulation with S0=0.75xKM.

Simulation of the time course for multiphosphorylation (Supplementary Fig. 3)

Simplified sequential mechanism

Simulation for Supplementary Fig. 3a
y(1) = S0; y(2) = S1P; y(3) = S2P; y(4) = S3P; y(5) = S4P; y(6) = S5P; y(7) = S6P;

k1=0.01; kcat/KM for S0 to S1P transition (for other sets of constant values see Supplementary Figure 3a)
k2=0.01; kcat/KM for S1P to S2P transition
k3=0.01; kcat/KM for S2P to S3P transition
k4= 0.01; kcat/KM for S3P to S4P transition
k5=0.01; kcat/KM for S4P to S5P transition
k6=0.01; kcat/KM for S5P to S6P transition

```
dydt = [-k1*y(1)
       k1*y(1)-k2*y(2)
       k2*y(2)-k3*y(3)
       k3*y(3)-k4*y(4)
       k4*y(4)-k5*y(5)
```

```
k5*y(5)-k6*y(6)
k6*y(6)];
```

The initial value for S0 was taken equal to 1, and it was assumed to be considerably below the K_M value.

Semiprocessive mechanism

For the set of constants see Fig. 3b

```
dydt = [(-k1-k2-k3-k4-k5-k6)*(1-y(2)-y(3)-y(4)-y(5)-y(6)-y(7))
      k1*y(1)-(k7+k8+k9+k10+k11)*y(2)
      k2*y(1)+k7*y(2)-(k12+k13+k14+k15)*y(3)
      k3*y(1)+k8*y(2)+k12*y(3)-(k16+k17+k18)*y(4)
      k4*y(1)+k9*y(2)+k13*y(3)+k16*y(4)-(k19+k20)*y(5)
      k5*y(1)+k10*y(2)+k14*y(3)+k17*y(4)+k19*y(5)-k21*y(6)
      k6*y(1)+k11*y(2)+k15*y(3)+k18*y(4)+k20*y(5)+k21*y(6)];
```

The initial value for S0 was taken equal to 1, and it was assumed to be considerably below the K_M value.

Supplementary discussion

Two RXL motifs were found to be responsible for Clb5 specificity for Sic1ΔC and full-length Sic1 (^{89}RTL^{91} and ^{114}RIL^{116}, designated as RXL2 and RXL3; Supplementary Fig. 4a, b). In cells overexpressing Sic1, mutations in these sites decreased viability and caused accumulation of cells with elongated buds, supporting the importance of hp/RXL-dependent Clb5 specificity in degradation of Sic1 (Supplementary Fig. 4c, d)[16]. The direct influence of the RXL mutations on the degradation rate of Sic1 in vivo was demonstrated using western blotting (Supplementary Fig. 4e). Mutation of the VLLPP motif, however, did not cause such toxic effects (Supplementary Fig. 4f), suggesting that Clb5-dependent phosphorylation is responsible for most degradation of Sic1. Additionally, the hp of Clb5 was found to be important for viability of cells overexpressing Sic1 (Supplementary Fig. 4g). These data are consistent with our other evidence that Cln2 is not the primary kinase responsible for phosphorylation of Sic1. Instead, they suggest that a major factor in Sic1 destruction is positive feedback created by the hp/RXL-enhanced and Clb5-dependent cooperative multisite phosphorylation of Sic1. The release of free Clb5-Cdk1 from stoichiometric inhibition using abrupt cooperative phosphorylation could be a powerful source of ultrasensitivity at the G1/S-transition.

In the time course experiments in Figure 2g, the steady-state levels of phosphorylated forms are not high, presumably because these forms are rapidly destroyed. This is most apparent in the case of the efficiently degraded forms of Sic1 (Sic1ΔC-7p and Sic1ΔC-7p-T48A). These data are not consistent with the original model of Sic1 degradation, according to which a graded Cdk1 signal is processed into an ultrasensitive switch via sigmoidally-accumulating multiphosphorylated species of Sic1. In fact, these multiphosphorylated species never accumulate because they are so rapidly phosphorylated and then ubiquitinated. Since intermediates do not accumulate in significant amounts, the signal response should correspond simply to the shape of the rising kinase signal, and there is not expected to be processing of a linear input into an ultrasensitive output. Instead, our data suggest that the source of ultrasensitivity and irreversibility at the G1/S transition is RXL/hp-dependent positive feedback driven by Clb5-Cdk1.

Supplementary references

25. Kito, K., Kawaguchi, N., Okada, S. & Ito, T. Discrimination between stable and dynamic components of protein complexes by means of quantitative proteomics. *Proteomics* **8**, 2366-2370 (2008).

26. Archambault, V. *et al*. Targeted proteomic study of the cyclin-Cdk module. *Mol. Cell* **14**, 699-711 (2004).

Supplementary Table 1

Docking constants (k_{dock}) determined for pairs of Cdk1 phosphorylation sites using Sic1ΔC mutants in which all but the indicated Cdk consensus sites are mutated to alanine. The k_{dock} values are defined as the ratio of the relative fraction of the doubly phosphorylated form and the enzyme activity units towards the specific N-terminal priming site present in the substrate. For experimental details see the legend of Figure 3 and the Supplemental Information. Values include the standard errors of the mean, calculated from at least two independent experiments. The nonconsensus Cdk site T48 was not mutated in these Sic1ΔC constructs and its phosphorylation was detectable only in the presence of T33 as the priming site (*).The pairs containing the site T2 were omitted, as T2 did not show any detectable additional impact on the coupling effects of the closely positioned site T5. The k_{dock} values for the two sites located further downstream (T173 and S191) were also excluded as these sites do not play crucial roles in Sic1 degradation and they did not exhibit any notable docking connection with the sites in the N-terminus.

Substrate	k_{dock} (relative units)		Substrate	k_{dock} (relative units)		Substrate	k_{dock} (relative units)	
	Cln2	Clb5		Cln2	Clb5		Cln2	Clb5
T5/T33	0.591±0.043	0.954±0.058	T33/T45	0.623±0.046	0.630±0.025	T45/T48*	0.01<	0.01<
T5/T45	0.475±0.026	0.480±0.111	T33/T48*	0.176±0.050	0.073±0.014	T45/S69	0.270±0.038	0.366±0.041
T5/T48*	0.01<	0.01<	T33/S69	0.052±0.018	0.092±0.008	T45/S76	0.536±0.082	0.916±0.079
T5/S69	0.052±0.003	0.096±0.010	T33/S76	0.267±0.047	0.518±0.064	T45/S80	0.135±0.038	0.583±0.032
T5/S76	0.423±0.007	0.689±0.107	T33/S80	0.039±0.011	0.520±0.070			
T5/S80	0.048±0.004	0.785±0.136						

Supplementary Table 2

Docking constants determined for selected pairs of Cdk1 phosphorylation sites in the context of mutated RXL2, RXL3 or VLLPP docking sites. The RXL-to-AXA or VLLPP-to-AAAAA mutations were introduced into the Sic1ΔC mutants containing pairs of sites (described in the Supplemental Information and in the legend of Supplementary Table 1).

Substrate	k_{dock} (relative units)		Substrate	k_{dock} (relative units)		Substrate	k_{dock} (relative units)	
	Cln2	Clb5		Cln2	Clb5		Cln2	Clb5
T5/T33-*3rx/*	0.701±0.039	1.062±0.144	T5/T33-*23rx/*	0.741±0.168	0.940±0.029	T5/T33-*vllpp*	0.125±0.016	0.963±0.022
T5/T45-*3rx/*	0.527±0.049	0.381±0.009	T5/T45-*23rx/*	0.376±0.012	0.063±0.011	T5/T45-*vllpp*	0.058±0.004	0.341±0.049
T5/S76-*3rx/*	0.431±0.001	0.197±0.033	T5/S76-*23rx/*	0.272±0.009	0.219±0.033	T5/S76-*vllpp*	0.055±0.005	0.468±0.029
T5/S80-*3rx/*	0.075±0.005	0.182±0.041	T5/S80-*23rx/*	0.042±0.006	0.187±0.024	T33/T45-*vllpp*	0.184±0.027	0.607±0.044
						T45/S76-*vllpp*	0.218±0.019	0.754±0.066

Supplementary Table 3

Yeast strains used in this study.

Strain	Description
DOM0076	gal-CLB5-TAP pRSAB1234 bar1:HISG sic1d::LEU2
DOM0077	gal-CLB2-TAP pRSAB1234 bar1:HISG sic1d::LEU2
DOM0957	gal-CLB3-TAP pRSAB1234 bar1:HISG sic1d::LEU2
DOM0963	gal-CLB5hpm-TAP pRSAB1234 bar1:HISG sic1d::LEU2
DOM0964	gal-CLB2hpm-TAP pRSAB1234 bar1:HISG sic1d::LEU2
MK0168	gal-CLB3hpm-TAP pRSAB1234 bar1:HISG sic1d::LEU2
DMY305	gal-CLN2-3HA
MK0172	clb5::clb5hpm bar1:HISG
MK0178	clb5::clb5hpm; clb6::clb6hpm bar1:HISG
MK0183	clb6::URA3 bar1:HISG
MK0184	clb5::clb5hpm; clb3::URA3 bar1:HISG
MK0186	clb5::clb5hpm; clb6::clb6hpm; clb3::URA3 bar1:HISG
DOM0090	bar1:HISG
DOM0856	clb5::URA3 bar1::HISG
MK0304	MK0172 [Sic1wt-3XHA-pRS413]
MK0305	MK0178 [Sic1wt-3XHA-pRS413]
MK0306	MK0183 [Sic1wt-3XHA-pRS413]
MK0307	MK0184 [Sic1wt-3XHA-pRS413]
MK0308	MK0186 [Sic1wt-3XHA-pRS413]
MK0309	DOM0856 [Sic1wt-3XHA-pRS413]
MK0158	Sic1wt-TAP:HISMX6 bar1:hiG
MK0166	Sic1wt::Sic1wt-*1234rxl*; Sic1wt-*1234rxl*-TAP HISMX6 bar1:hisG
MK0311	Sic1wt::Sic1wt-*vllpp*; Sic1wt-*vllpp*-TAP HISMX6 bar1:hisG
MK0312	Sic1wt-TAP:HISMX6 [pGAL-Sic1ΔN-Ylplac211] bar1:hiG
MK0313	Sic1wt::Sic1wt-T48+1P/S69+2R/S80+2R; Sic1wt- T48+1P/S69+2R/S80+2R-TAP HISMX6 bar1:hisG
MK0314	Sic1wt::Sic1wt-T48+1P/S69+2R/S80+2R; Sic1wt- T48+1P/S69+2R/S80+2R-TAP HISMX6 [pGAL-Sic1ΔN-Ylplac211] bar1:hisG
MK0315	CLN2-3HA HISMX6 [pGAL-Sic1ΔN-Ylplac211] bar1:hisG
MK0316	CLB5-3HA HISMX6 [pGAL-Sic1ΔN-Ylplac211] bar1:hisG
MK0317	MK0158 pGALL-Cks1 KanMX
MK0318	MK0317 [pRS315]
MK0319	MK0317 [Cks1-wt-pRS315]
MK0320	MK0317 [Cks1-R33E/S82E/R102A-pRS315]
MK0321	MK0267 [pRSAB1234]
MK0322	[pRS413] [Cks1-wt-pRSAB1234]
MK0323	MK0267 [Cks1-wt-pRSAB1234]
MK0324	MK0267 [Cks1R33E/S82E/R102A-pRSAB1234]
MK0325	[pRS413] [Cks1R33E/S82E/R102A-pRSAB1234]

Supplementary Table 4

Plasmids used in this study.

Plasmid	Description	Plasmid	Description
pMK0092-0097	Sic1AP-T33-ΔC-pET28a and *rxl* variants	pMK0182	Sic1AP-T173/S69/S76/S80-ΔC-pET28a
pMK0098-0103	Sic1AP-S76-ΔC-pET28a and *rxl* variants	pMK0183	Sic1AP-S191/S69/S76/S80-ΔC-pET28a
pMK0108-0113	Sic1AP-T2-ΔC-pET28a *rxl* variants	pMK0191	Sic1wt-*vllpp*(136AAAAA140)-ΔC-pET28a
pMK0114-0119	Sic1AP-T5-ΔC-pET28a *rxl* variants	pMK0198	Sic1AP-T33/T45/T48A-ΔC-pET28a
pMK0120-0125	Sic1AP-T45-ΔC-pET28a *rxl* variants	pMK0500	Sic1wt-3XHA-pRS413
pMK0126-0131	Sic1AP-S69-ΔC-pET28a *rxl* variants	pMK0501	Sic1AP-3XHA-pRS413
pMK0132-0137	Sic1AP-S80-ΔC-pET28a *rxl* variants	pMK0502	Sic1wt-*1234rxl*-3XHA-pRS413
pMK0138-0143	Sic1AP-T173-ΔC-pET28a *rxl* variants	pMK0504	Sic1wt-*23rxl*-3XHA-pRS413
pMK0144-0149	Sic1AP-S191-ΔC-pET28a *rxl* variants	pMK0505	Sic1wt-*14rxl*-3XHA-pRS413
pMK0150	Sic1wt-ΔC-pET28a	pMK0505	Sic1AP-T33/T45/S69/S76/S80-3XHA-pRS413
pMK0151	Sic1wt-ΔC-*234rxl* -pET28a	pMK0506	Sic1AP-T33/T45/T48A/S69/S76/S80-3XHA-pRS413
pMK0152	Sic1wt-ΔC-*134rxl* -pET28a	pMK0507	Sic1AP-T33/T45/T47-T49AAA/S69/S76/S80-3XHA-pRS413
pMK0153	Sic1wt-ΔC-*124rxl* -pET28a	pMK0508	Sic1AP-T33/S69/S76/S80-3XHA-pRS413
pMK0154	Sic1wt-ΔC-*123rxl* -pET28a	pMK0509	Sic1AP-T33/T45/S69/S76-3XHA-pRS413
pMK0155	Sic1wt-ΔC-*1234rxl* -pET28a	pMK0510	Sic1AP-T33/T45/S76/S80-3XHA-pRS413
pMK0156	Sic1wt-ΔC-*1rxl* -pET28a	pMK0511	Sic1wt-T48A-3XHA-pRS413
pMK0157	Sic1wt-ΔC-*2rxl* -pET28a	pMK0512	Sic1wt-S69A-3XHA-pRS413
pMK0158	Sic1wt-ΔC-*3rxl* -pET28a	pMK0513	Sic1wt-S80A-3XHA-pRS413
pMK0159	Sic1wt-ΔC-*4rxl* -pET28a	pMK0514	Sic1AP-T33/T45/S76-3XHA-pRS413
pMK0160	Sic1AP-T5/T33-ΔC-pET28a	pMK0515	Sic1wt-*1234rxl*-T48+1P/S69+2R/S80+2R-3XHA-pRS413
pMK0161	Sic1AP-T5/T45-ΔC-pET28a	pMK0518	Sic1AP-S69/S76/S80-3XHA-pRS413
pMK0162	Sic1AP-T5/S69-ΔC-pET28a	pMK0519	Sic1AP-T5/S69/S76/S80-3XHA-pRS413
pMK0163	Sic1AP-T5/S76-ΔC-pET28a	pMK0520	Sic1AP-T33/S69/S76/S80-3XHA-pRS413
pMK0164	Sic1AP-T5/S80-ΔC-pET28a	pMK0521	Sic1AP-T45/S69/S76/S80-3XHA-pRS413
pMK0165	Sic1AP-T33/T45-ΔC-pET28a	pMK0522	Sic1AP-T2/S69/S76/S80-3XHA-pRS413
pMK0166	Sic1AP-T33/S69-ΔC-pET28a	pMK0527	Sic1wt-*vllpp*-3XHA-pRS413
pMK0167	Sic1AP-T33/S76-ΔC-pET28a	pMK0535	Sic1wt-S9A-3XHA-pRS413
pMK0168	Sic1AP-T33/S80-ΔC-pET28a	pMK0536	Sic1wt-S69A/S80A-3XHA-pRS413
pMK0169	Sic1AP-T45/S69-ΔC-pET28a	pMK0537	Sic1wt-ΔC-3XHA-pRS315
pMK0169	Sic1AP-T45/S76-ΔC-pET28a	pMK0538	Sic1wt-T48A-ΔC-3XHA-pRS315
pMK0169	Sic1AP-T45/S80-ΔC-pET28a	pMK0539	Sic1AP-T2/T5/T33/T45/S76-ΔC-3XHA-pRS315
pMK0170	Sic1AP-T5/T33-ΔC-*1234rxl* -pET28a	pMK0540	Sic1AP-T2/T5/T33/T45/T48A/S76-ΔC-3XHA-pRS315
pMK0171	Sic1AP-T5/T45-ΔC-*1234rxl* -pET28a	pMK0541	Sic1wt-*1234rxl*-T48+1P-3XHA-pRS413
pMK0172	Sic1AP-T5/S69-ΔC-*1234rxl* -pET28a	pMK0542	Sic1wt-*1234rxl*-S69+2R-3XHA-pRS413
pMK0173	Sic1AP-T5/S76-ΔC-*1234rxl* -pET28a	pMK0543	Sic1wt-*1234rxl*-S80+2R-3XHA-pRS413
pMK0174	Sic1AP-T5/S80-ΔC-*1234rxl* -pET28a	pMK0544	Sic1wt-*1234rxl*-T48+1P/S69+2R/S80+2R-3XHA-pRS413
pMK0175	Sic1AP-T33/T45-ΔC-*1234rxl* -pET28a	pMK0546	pGAL1-Sic1ΔN-Yplac211
pMK0176	Sic1AP-T33/S76-ΔC-*1234rxl* -pET28a	pMK0547	Sic1wt-T48A/S69A/S80A-3XHA-pRS413
pMK0177	Sic1AP-T45/S76-ΔC-*1234rxl* -pET28a	pMK0548	Cks1-wt-pRS315
pMK0178	Sic1AP-T2/T5/S69/S76/S80-ΔC-pET28a	pMK0549	Cks1-R33A/S82E/R102A-pRS315
pMK0179	Sic1AP-T5/S69/S76/S80-ΔC-pET28a	pMK0550	Cks1-wt-pRS1234
pMK0180	Sic1AP-T33/S69/S76/S80-ΔC-pET28a	pMK0551	Cks1-R33E/S82E/R102A-pRS1234
pMK0181	Sic1AP-T45/S69/S76/S80-ΔC-pET28a		

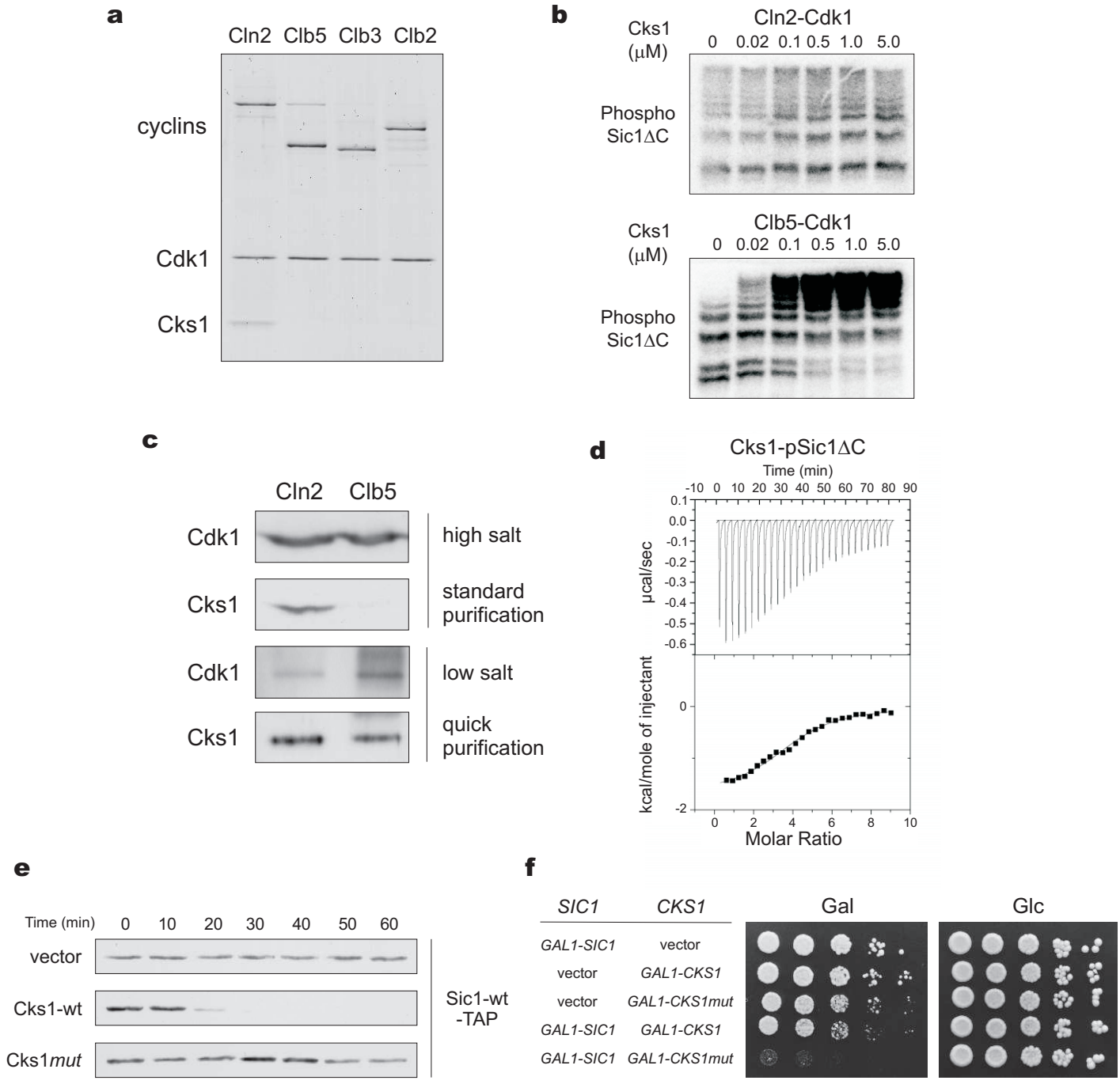

Supplementary Figure 1. Evaluation of in vivo stoichiometry of Cks1 in cyclin-Cdk1 complexes and of the ability of Cks1 to bind phosphorylated Sic1ΔC. (a) Cln2- and Clb-Cdk1 complexes were purified from yeast strains carrying TAP-tagged (Clbs) or 3HA-tagged (Cln2) cyclin. This figure shows a Coomassie Blue-stained gel of the preparations. Purified Cln2-Cdk1 contained about equal amount of Cks1 and Cdk1, while the Clb5-Cdk1 complex contained no detectable Cks1. (b) The ability of Cks1 to promote processive phosphorylation of Sic1ΔC was studied using different concentrations of Cks1 in phosphorylation assays with Cln2- and Clb5-Cdk1 preparations. Multiphosphorylated forms were separated using Phos-Tag SDS-PAGE. The concentration of Cks1 required for half-maximal enhancement was found to be ~150 nM for Clb5-Cdk1, while the Cln2-Cdk1 complex did not require any added Cks1. These results confirm that the purified Cln2-Cdk1 complex, but not the Clb5-Cdk1 complex, is fully occupied by Cks1. The concentration of Cln2 was taken lower compared to the Fig 1a-e to follow the initial processivity profile which is the most sensitive range with respect to the Cks1 effect. (c) The relatively low Cks1 concentration required for the half-maximal stimulation of Clb5-Cdk1 in panel (b) might suggest that Clb5-Cdk1 is saturated with

Legend of Supplementary Figure 1 (continued)

Cks1 inside the cell. As the standard TAP purification of cyclin-Cdk1 complexes includes a high salt concentration in the lysis and washing buffers, as well as long purification times (several hours), a substantial fraction of Cks1 may dissociate from the Clb5-Cdk1 complex. To test this possibility, Cln2-3HA-Cdk1 and Clb5-3HA-Cdk1 were isolated either in the presence of high salt (1 M NaCl, standard purification protocol, several hours) or low salt (0.1 M NaCl, quick purification protocol, 45 minutes), using immunoaffinity chromatography with anti-HA polyclonal antibody. The resulting preparations were analyzed by western blotting with anti-Cdk1 and rabbit anti-Cks1 antibodies, as shown here. The results with the quick purification protocol suggest that the relative amount of Cks1 that remained attached to the Clb5-Cdk1 complex was only slightly less than in the case of Cln2-Cdk1. The conclusion that both Cln2-Cdk1 and Clb5-Cdk1 complexes have high Cdk1:Cks1 stoichiometry is also supported by previous reports. A recent study using the quantitative SILAC method reported that Clb-Cdks have at least 50% of Cks1 stoichiometrically bound [25]. Additionally, several proteomics studies on cyclin-Cdk1 complexes have reported Cks1 to be bound to the Clb5-Cdk1 complex, which again, considering the off-rate and the time of complex isolation, suggests high stoichiometry in the cellular environment [26]. Our observation that the Cln2-Cdk1 complex has a higher affinity for Cks1 is also consistent with previous evidence that Cln2-Cdk1 is more dependent on Cks1 than Clb-Cdk1 for kinase activity [12]. (d) The affinity of phospho-Sic1ΔC for Cks1 was analyzed by isothermal titration calorimetry. The K_D for the fully phosphorylated Sic1ΔC is 11$\pm$2 μM, while the non-phosphorylated version of Sic1ΔC does not show any detectable binding (not shown). The stoichiometry of binding (n) is 3.5$\pm$0.8 molecules of Cks1 per molecule of pSic1ΔC, suggesting that Cks1 can bind multiple phosphorylated sites. (e) Effect of a phosphate-binding pocket mutant of Cks1 (Cks1mut) on the degradation of endogeneous Sic1. Cells expressed the Cks1-wt or Cks1mut from a CEN/ARS vector under the ADH promoter, and the endogeneous copy of CKS1 was under the control of the GALL promoter. Cells were grown and maintained on galactose plates and transferred to glucose-containing liquid media and grown to OD_{600}=0.2-0.6 to downregulate the endogenously expressed Cks1-wt. Cells carrying an empty vector or Cks1mut showed slower growth rate and elongated buds, but no arrest (data not shown). Cells were arrested in G1 using 2.5 h treatment with α-factor, after which the α-factor was removed and endogeneous Sic1 levels were followed by western blotting. In cells carrying wild-type Cks1-wt, Sic1 protein disappeared at a normal rate, while Sic1 was stabilized in the absence of Cks1 or in cells expresssing Cks1mut. (f) Viability assay showing the importance of the Cks1 phosphate-binding pocket for degradation of Sic1. Cells in this experiment expressed Sic1-wt from a CEN/ARS vector under the GAL1 promoter, plus either Cks1-wt or Cks1mut under the GAL1 promoter on a 2-micron plasmid. Expression of Cks1mut severely suppressed the growth of Sic1-overexpressing cells, supporting the notion that the phosphate-binding pocket of Cks1 is responsible for efficient phosphorylation and degradation of Sic1 in vivo.

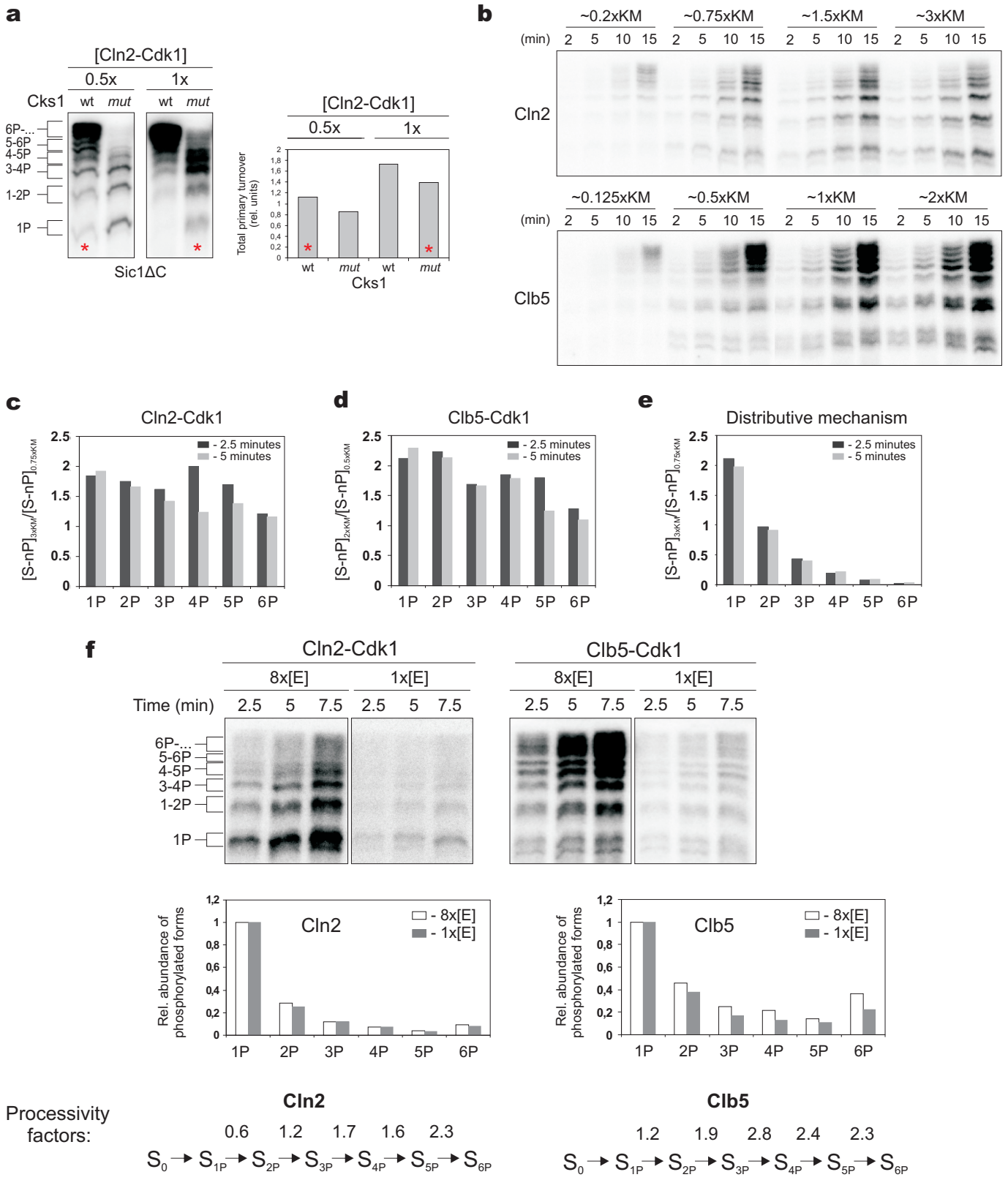

Supplementary Figure 2. Analysis of the processivity of Sic1ΔC multiphosphorylation. (a) Comparison of Sic1ΔC phosphorylation patterns at different enzyme concentrations and in the presence and the absence of Cks1mut. Two-fold differences in enzyme concentration were used in two parallel assays; note that the data with 0.5X enzyme concentration are the same as those shown in Fig. 1a. The total amounts of primary substrate turnover were calculated by summing the concentrations of multiply phosphorylated species and dividing the intensities of individual bands by the number of phosphates, as indicated on the left side of the figure. These values (plotted at right) express the relative number of Sic1 molecules modified, regardless of the number of phosphates added to one molecule. As an example, the asterisks illustrate how the degree of multiphosphorylation in the autoradiogram can decrease in the mutant even

Legend of Supplementary Figure 2 (continued)

though the amount of substrate turnover changes very little, confirming that the effect of Cks1mut is to switch the process from a processive to a distributive mode of phosphorylation. (b) Sic1∆C phosphorylation by Cln2-Cdk1 or Clb5-Cdk1 was analyzed at different Sic1∆C concentrations relative to apparent K_M values. (c, d) Data for each of the multi-phosphorylated isoforms from the experiment in panel (b) were plotted as the ratios of the values obtained at the indicated two substrate concentrations, at the two first time points of the experiments. (e) Values for similar time points as in (c) and (d), obtained from a simulation of a phosphorylation time course for a simple multistep phosphorylation system with a distributive mechanism. The system of equations used for the simulation is presented in the Supplementary Equations section. In the case of the distributive mechanism, at higher S0 values, the inhibitory term $1+S_0/K_M$ suppresses each subsequent step of the cascade, resulting in the declining profile. By using the processive mechanism, the enzyme can reduce the inhibitory pressure of the competing S0 at every step and make the pattern closer to horizontal, as shown in our data with Cln2 and Clb5. (f) Analysis of the processivity of Sic1∆C multiphosphorylation using different enzyme dilutions, showing the early formation of multiphosphorylated forms at different enzyme dilutions. The time points were taken at low levels of phosphorylation (less than 3% of total turnover), so that the quasi-steady states of the intermediate forms were not yet reached. Histograms below the autoradiographs show the relative abundance of phosphorylated species, quantified from the first time points (Clb5) or the third time points (Cln2) in the experiments shown above. The intensities of the ^{32}P-labeled bands were divided by the number of phosphates as indicated. Compared to the experiments presented in Fig. 1a, b, d and Supplementary Fig. 2a less enzyme was used to follow only the early events of the multiphosporylation process and more radioactive ATP was used to better visualize the weak signals of these early time points. To probe the processivity of the mechanism, two different enzyme dilutions were used. In the case of a processive reaction, the relative abundances of phosphorylated isoforms at early time points should not depend on enzyme concentration. Thus, the experiment shown here reveals a considerable level of processivity with Cln2 and Clb5. The processivity factors reflecting the probability of the next processive step versus the dissociation of the enzyme from the complex with an intermediately phosphorylated form were calculated for each subsequent phosphorylation event as a ratio of the sum of intensities of all forms with higher number of phosphates than the given phosphorylated form and the intensity of the given phosphorylated form itself.

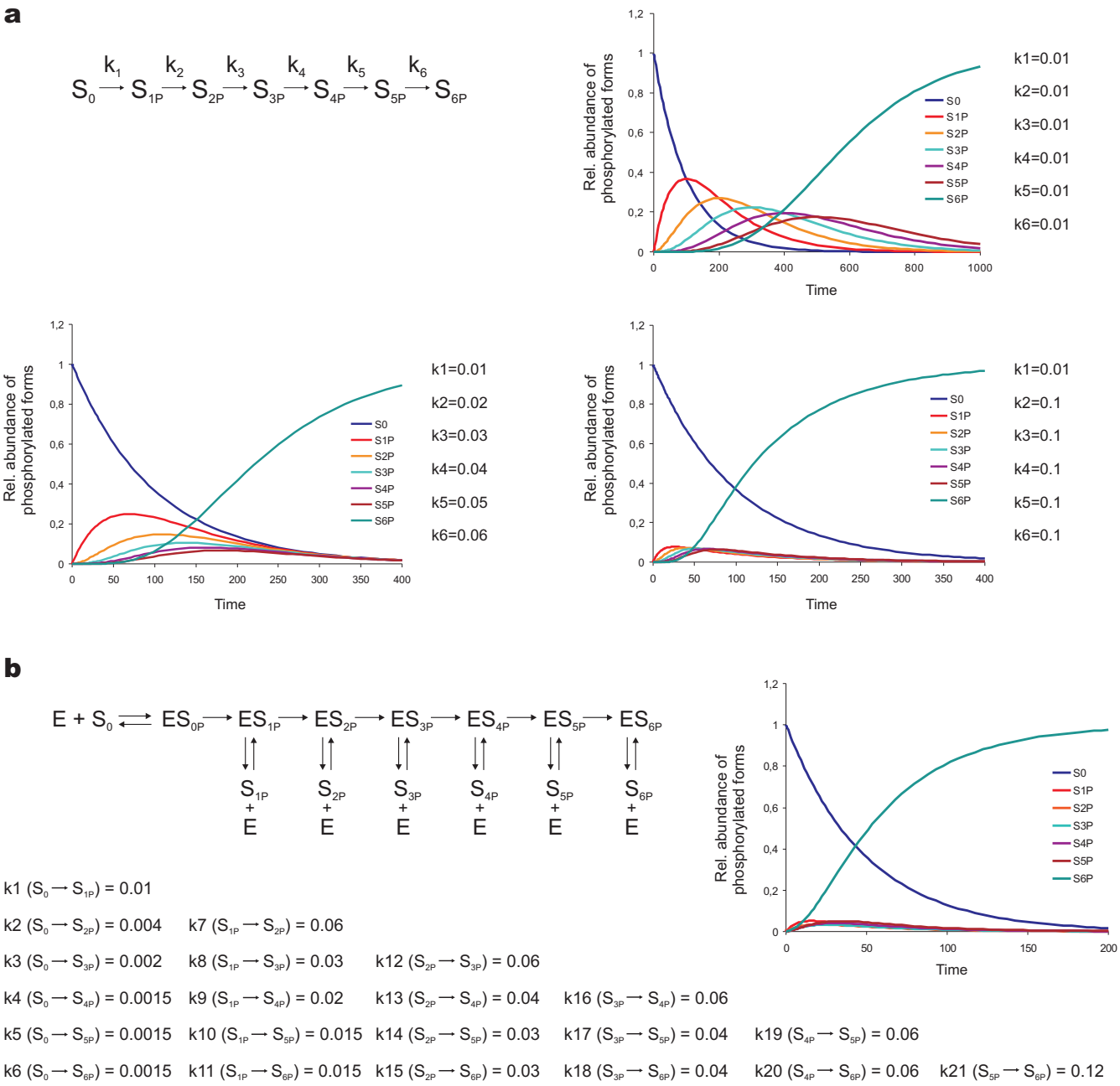

Supplementary Figure 3. Simulation of the multiphosphorylation time courses. Ordinary differential equation (ODE) models with different sets of constants were used to simulate the shapes of plausible time courses for multisite phosphorylation. For the ODE systems see the Supplementary Equations section. (a) Phosphorylation time courses based on a simplified sequential phosphorylation process with different sets of individual rate constants, as shown to the right of the graphs, were simulated to follow the dynamics of different phosphorylated forms. The upper right panel presents a simulation of a process with equal rates for each individual step. In this case, there is a considerable temporal accumulation of intermediates and the levels of these intermediates are in a range that is comparable to the levels of S0 and S6P. This is the opposite of the time course patterns shown in Fig. 1d and e, where the steady-state levels of the intermediately phosphorylated forms are well below the levels of S0 and S6P during the mid-section of the time course (compare the height of the intersection point of S0 and S6P with the quasi-steady-state levels of the intermediates). The lower left panel presents a process with gradually increasing rates for the individual steps. In this case, the quasi-steady-states are accumulating less than in the previous simulation, but the levels of these states are less overlapping. Again, this pattern does not resemble

Legend of Supplementary Figure 3 (continued)

closely that obtained in the experiment presented in Fig. 1d and e. The lower right panel presents a simulation with a slower initial priming step and fast secondary steps. Except the lag of S6P, this time course matches quite closely the experimental time courses given in Fig. 1d and e, suggesting that phosphorylation of Sic1 begins with a slow Cks1-independent priming step followed by fast phosphate-docking steps. (b) Although the time course in lower right panel of (a) matches already quite well with the experimental time courses and includes a sequence of slow (Cks1-independent) and fast (Cks1-dependent) steps, it is a simplified ordered system and does not include processivity. Since the mechanism was experimentally shown to include processivity, we aimed to combine the findings presented in Fig. 1e and Supplementary Fig. 2b-f with the time course simulations in panel (a) above and created a model that simulates the processivity of the enzyme. For a processive enzyme, there exist two possibilities at every step: the enzyme either dissociates from the intermediately-phosphorylated substrate or it exchanges ADP for ATP and adds another phosphate to the next site. The net outcome of such a mechanism is that, in principle, every multiphosphorylated form can be formed directly over one or more processive steps from any forms with fewer phosphates. Based on the kinetic scheme shown in panel (b), above left, and taking into account the range of relative processivity factors estimated in the experiment in Supplementary Fig. 2f, we constructed a time course simulation model for processive multiphosphorylation using the set of constants presented in panel (b). The simulated data at right even more precisely matched those obtained in the experiments presented in Fig. 1d and e, further suggesting that multiphosphorylation of Sic1 follows Cks1-dependent processive mechanism. Importantly, the processive simulation reduced the lag of S6P formation compared to the simulations in panel (a). Similar, almost immediate, start of the accumulation of S6P was observed also in the experiment, suggesting that a considerable fraction of the S6P is formed processively, without the formation of quasi steady states of the intermediates.

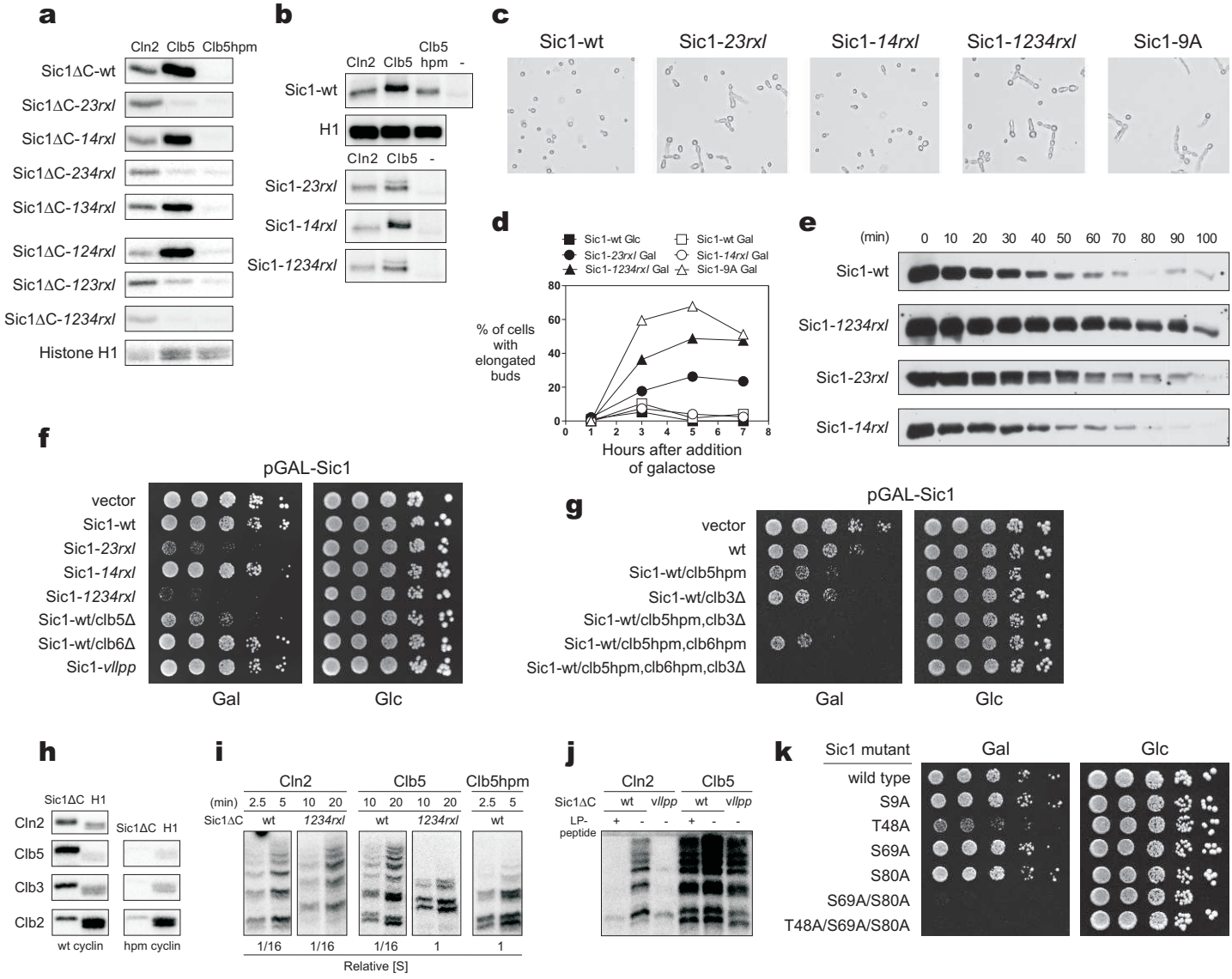

Supplementary Figure 4. Analysis of Sic1 phosphorylation and degradation. (a) Mapping of two RXL motifs responsible for efficient phosphorylation of Sic1ΔC by Clb5-Cdk1. (b) Phosphorylation of full-length wild-type Sic1 and versions with mutated RXL motifs, bound in an inhibitory complex with Clb5-TAP-Cdk1. An extract containing overexpressed Clb5-TAP was applied to IgG beads. After binding and washing, an excess amount of purified Sic1 was loaded to fully saturate and inhibit the bound Clb5-Cdk1 complex. Kinase reactions were started by adding purified Cln2- or Clb5-Cdk1 and ^{32}P-ATP to the mixture containing the bead suspension carrying the inhibitory complex. The data reveal that the RXL-docking specificity of full-length Sic1 in the inhibitory complex is the same as that observed in solution with Sic1ΔC, confirming that Sic1ΔC is a valid model for the specificity studies. (c, d) Accumulation of arrested cells with elongated buds after the induction of Sic1-23rxl and Sic1-1234rxl expression with galactose. Strains expressing Sic1-wt and Sic1-14rxl were used as controls. The nondestructible mutant with all 9 Cdk1 sites mutated to alanines (Sic1-9A) was also used as a control. (e) Western blotting analysis of Sic1 degradation in vivo. Cells carrying Sic1-wt, Sic1-23rxl, and Sic1-1234rxl under the GAL1 promoter in CEN vectors were synchronized in hydroxyurea for 2.5 h. Galactose was added for 45 min and cells were released from the arrest into media lacking hydroxyurea and galactose. Sic1 levels were followed by the detection of the C-terminal 3HA. (f) Galactose plate assay to test the importance of RXL docking sites, the VLLPP docking site, and S-phase cyclins Clb5 and Clb6 in degradation of Sic1. (g) A requirement for the hydrophobic patch of Clb5 for suppression of Sic1 function. Deletion of Clb3 enhanced the requirement for Clb5, probably because Clb3hpm-Cdk1 was not significantly inhibited by Sic1 (Ki,Sic1/Clb3hpm=1.7 μM compared to Ki,Sic1/Clb3wt=1.0 nM). Thus, the ability of Clb3-Cdk1 to use hydrophobic patch-dependent phosphorylation of Sic1 is likely to be sufficient to compensate for the effect of the hpm mutation of Clb5.

Legend of Supplementary Figure 4 (continued)

(h) Phosphorylation of Sic1ΔC was measured using equimolar amounts of four representative cyclin-Cdk1 complexes (Cln2-Cdk1, Clb5-Cdk1, Clb3-Cdk1, and Clb2-Cdk1) or hydrophobic patch mutants (hpm) of the Clb-Cdk1 complexes. Histone H1 was added as a control and standard SDS-PAGE was used. (i) Cln2-Cdk1, Clb5-Cdk1, or Clb5hpm-Cdk1 kinase complexes were used in a phosphorylation assay with Sic1ΔC and Sic1ΔC-1234rxl (the R and L residues mutated to A in all four RXL motifs). Different substrate concentrations (below K_M) and two time points were chosen to have nearly equal primary turnovers of the first phosphorylation step, allowing a better comparison of processivity profiles. Thus, the total phosphorylation signals in this experiment do not reflect relative net specificities between Clb5-Cdk1 and Cln2-Cdk1. (j) The effect of the Cln2-specific docking motif VLLPP on the phosphorylation dynamics of Sic1ΔC by Cln2- or Clb5-Cdk1 was studied using the competitor peptide VLLPPSRPTS based on the sequence of the Cln2-specific docking site and a Sic1ΔC version with the VLLPP docking site mutated to alanines (Sic1ΔC-vllpp). (k) The nonconsensus Cdk1 site T48 is important for viability of cells overexpressing Sic1. In this panel, only the indicated sites are mutated and all other sites remain unchanged. Mutation of the nonconsensus Cdk site S9 in the predicted pT5/pS9 degron had no effect, and the other suboptimal Cdk sites of predicted degrons pS69/pS76 and pS76/pS80 (S69 and S80) did not have any effect when mutated alone.

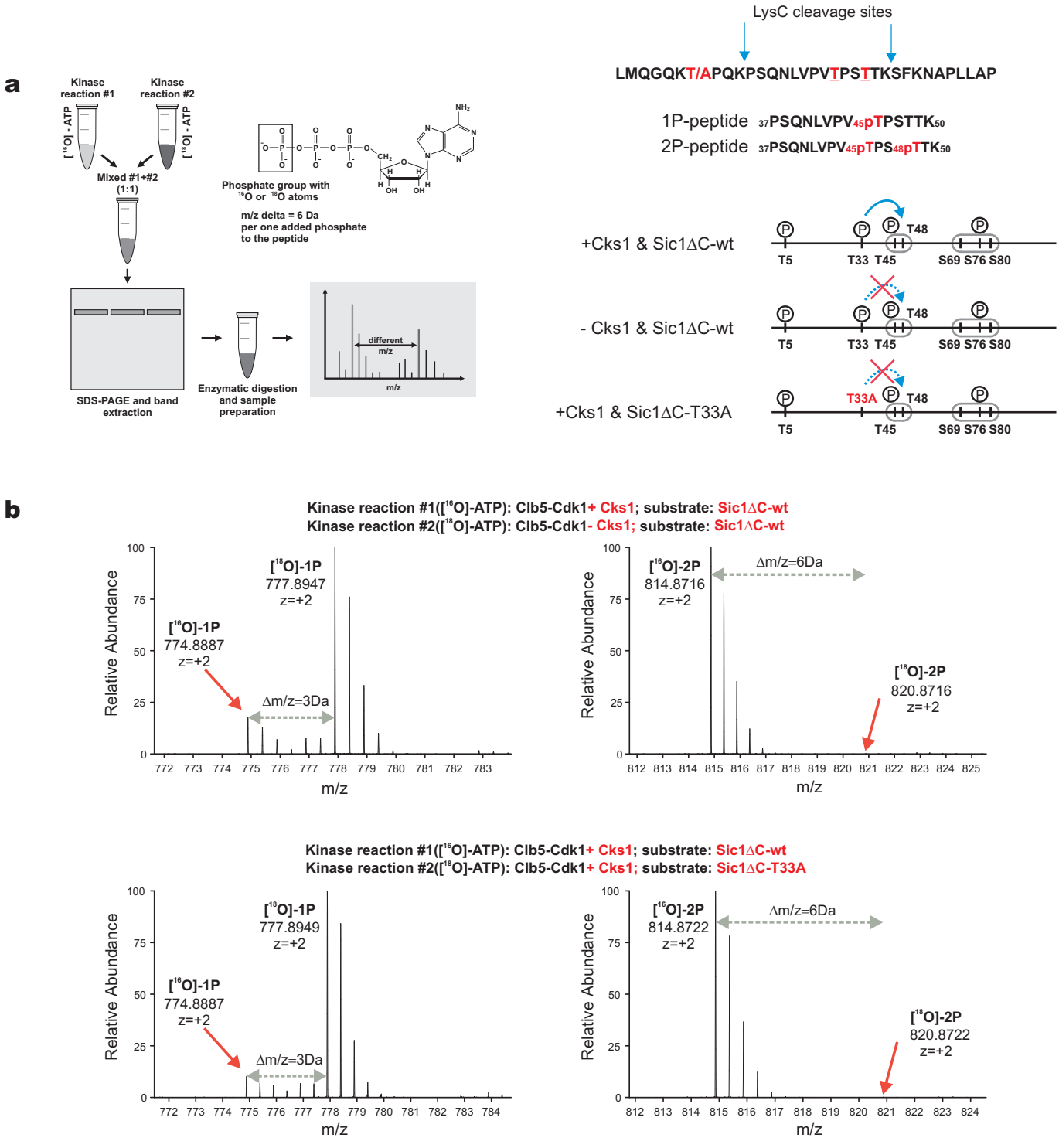

Supplementary Figure 5. Analysis of Cks1-dependent phosphorylation of the 'non-Cdk' site T48 using quantitative mass-spectrometry. The aim of the experiment was to demonstrate that the phosphorylation of T48 is dependent on Cks1, and secondly, that the presence of the priming site T33 is required. The first pair of assays was performed using Sic1ΔC-wt and Clb5-Cdk1 in the presence and absence of Cks1. The second pair of assays was designed to compare the Clb5-dependent phosphorylation of Sic1ΔC-wt and Sic1ΔC-T33A as substrates in the presence of Cks1. (a) A schematic view of the procedure. The two kinase reactions to be quantitatively compared were performed according to the standard kinase assay protocol with the exception that one of the reactions contained heavy [18O]-ATP instead of the ordinary ATP. After stopping the reactions at different time points the contents of the tubes were mixed and subjected to SDS-PAGE. Coomassie-stained bands corresponding to Sic1ΔC and Sic1ΔC-T33A were

Legend of Supplementary Figure 5 (continued)

excised and submitted to LysC-catalyzed proteolytic cleavage. The resulting peptide mixtures were analyzed by tandem mass spectrometry and the relative intensities of the 'heavy' and 'light' phosphopeptides were compared. The right side of panel (a) shows the sequence of the LysC-generated peptide corresponding to the region of interest in Sic1. Both singly (1P) and doubly (2P) phosphorylated forms of this peptide were detected in MS analysis, and based on the fact that T45 is the only Cdk1 consensus site (also mapped to be the site efficiently phosphorylated by Cdk1 (Figure 2b)), it was inferred that the 1P peptide contained the phosphorylated pT45 and the 2P peptide contained the phosphorylated pair of pT45/pT48. The stoichiometric phosphorylation of T45 and T48 (and not the other S or T residues) in this region of Sic1 has also been reported in a previous study [7]. (b) Examples of MS spectra showing the relative intensities of the phosphopeptides estimated from the 60 minute reaction time point.The positions of the peptides with the 3 Da (1P) and 6 Da (2P) isotope shifts are shown. Both the T33A mutation and the absence of Cks1 caused a major decrease in the phosphorylation of T48; in fact, the peptide was undetectable in the background, suggesting that T33 and Cks1 may potentiate T48 phosphorylation rate over a thousand-fold.

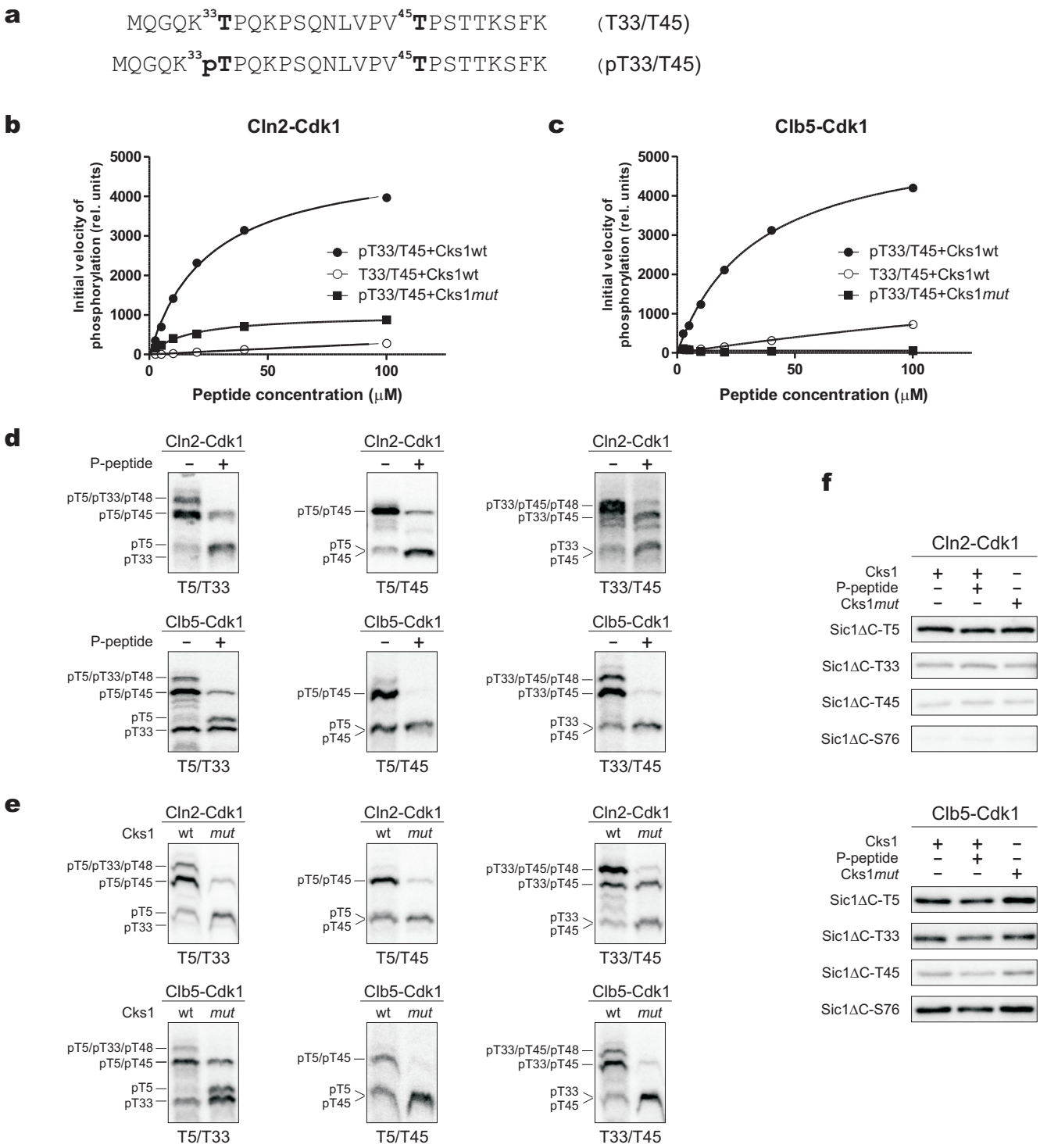

Supplementary Figure 6. Phosphorylation-dependent enhancement of secondary phosphorylation steps in substrate constructs containing two phosphorylation sites. (a) Synthetic peptide substrates based on the sequence around the Cdk consensus sites T33/T45 in Sic1, and containing either the unphosphorylated or phosphorylated threonine at position 33. (b, c) Michaelis-Menten curves showing the importance of primary phosphorylation at position T33 for the phosphorylation of the peptide substrates presented in (a). The K_M values for the pT33/T45 peptide were 21.0±3.2 μM and 33.4±2.2 μM for Cln2- and Clb5-Cdk1, respectively. To demonstrate the importance of Cks1 for the phosphorylation-dependent docking effect, control reactions with Cks1mut were performed for the pT33/T45 peptide. The weaker effect of the Cks1mut in reactions with Cln2-Cdk1 can be explained by the relatively high affinity of Cks1 for the Cln2-Cdk1 complex (Supplementary Fig. 1b and c), which is expected to reduce exchange of the mutant for the endogenous wild-type Cks1. (d, e) Phosphorylation of Sic1ΔC mutants containing just two of the Cdk phosphorylation sites in the presence of wild-type Cks1 and phosphorylated competitor peptide (pT45) (d) or Cks1mut (e). Phos-Tag SDS-PAGE was used to separate different phosphorylated forms. (f) Phosphorylation of Sic1ΔC mutants containing just a single Cdk phosphorylation site in the presence of wild-type Cks1, phosphorylated competitor peptide (pT45) or Cks1mut.

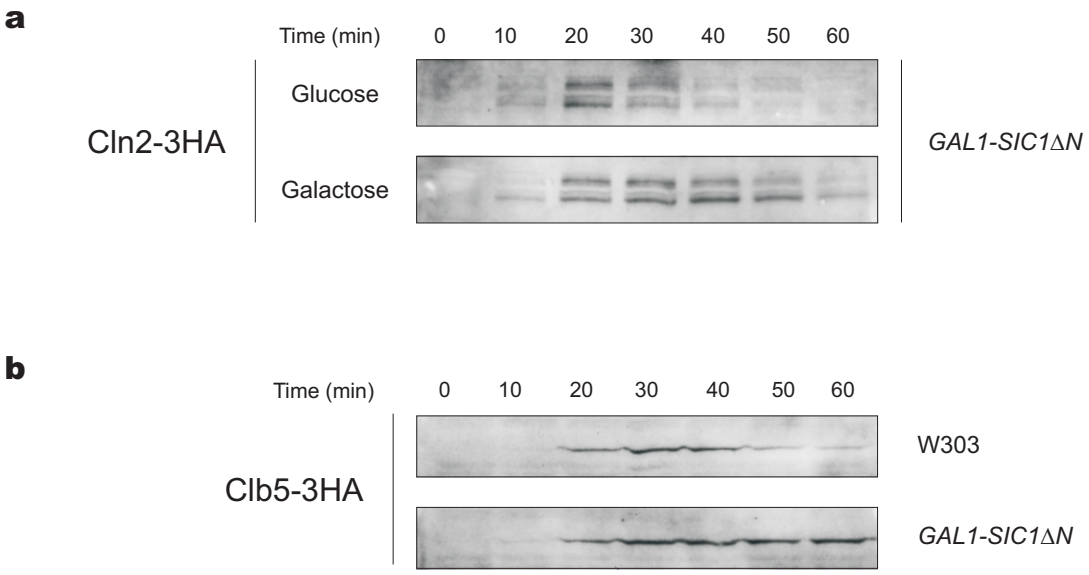

Supplementary Figure 7. Effects of Sic1ΔN overexpression on levels of Cln2 and Clb5. (a) Analysis of Cln2-3HA protein levels after induction of the nondegradable inhibitory domain of Sic1 (SIC1ΔN) from the galactose promoter (lower panel). As a control, the same experiment was performed with the addition of glucose (upper panel). (b) Analysis of the levels of Clb5-3HA in a similar experiment to that presented in Fig. 3f, showing that overexpression of Sic1ΔN does not affect the timing of the initial rise of Clb5 protein. Given the fact that the transcription of CLB5 is directly dependent on Cln-Cdk1 activity, these data confirm that Cln-Cdk1 activity is unaffected by the overexpression of Sic1ΔN. Additionally, in the case of Clb5-Cdk1, the K_i value for the purified Sic1ΔN was in the low nanomolar range (1.7 nM) and similar to that for wild-type Sic1, but no significant inhibition of Cln2-Cdk1 was observed even at 200 micromolar concentrations of Sic1ΔN (data not shown), confirming that Cln-Cdk1 activity is not influenced by the overexpression of Sic1ΔN. Longer time courses in these experiments revealed that Sic1 levels eventually decline with a half life of 2-3 hours, compared to a few minutes in cells freely expressing Clbs (data not shown). These data are in agreement with our in vitro results suggesting that Cln2 can finalize the phosphorylation cascade, but due to the slow last steps it may take several hours to overcome the threshold.

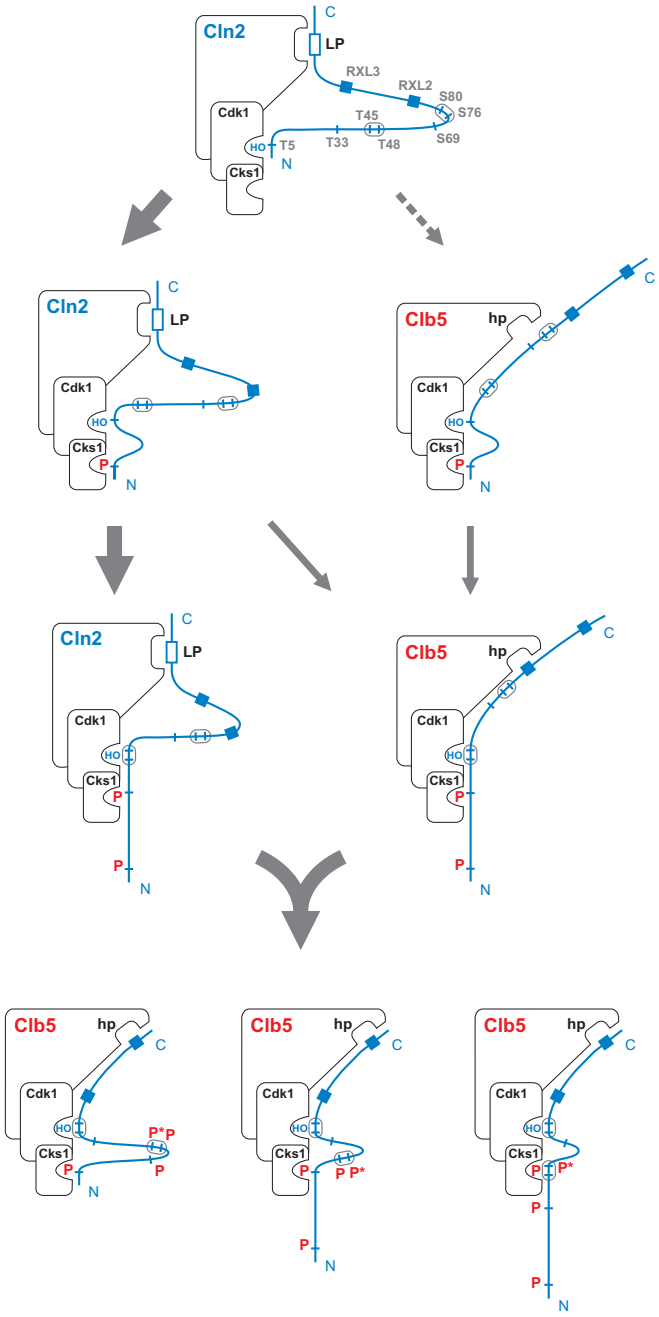

Supplementary Figure 8. A schematic diagram describing the prevalent routes of Cln2- and Clb5-dependent multi-phosphorylation of Sic1. The optimal positioning of phosphorylation sites and docking motifs in the substrate is defined by the positioning of the three docking pockets: Cks1, active site, and docking sites in cyclins (hp in Clb5 and the putative docking site for VLLPP motif in Cln2). Since Sic1 is an intrinsically disordered protein, the optimal positioning of docking motifs and phosphorylation sites could be directly proportional to the distances corresponding to the length of the peptide chains between these sites. We propose that the cascade starts with the Cln2-dependent phosphorylation of sites in the N-terminus (T5 or T33). Phosphorylated sites would then serve as priming sites for Cks1-dependent phosphorylation of downstream sites (T33, T45 and S76) and of the nonconsensus Cdk site T48 (P*). The emerging Clb5-dependent feedback loop will continue the cascade from different phosphorylated species.